Langmuir Article

pubs.acs.org/Langmuir

Elemental Depth Profiling of Fluoridated Hydroxyapatite: Saving Your Dentition by the Skin of Your Teeth?

Frank Müller,*[,†] Christian Zeitz,[†] Hubert Mantz,[†] Karl-Heinz Ehses,[†] Flavio Soldera,[‡] Jörg Schmauch,[§] Matthias Hannig,[∥] Stefan Hüfner,[†] and Karin Jacobs[†]

[†]*Experimental Physics,* [‡]*Functional Materials, and* [§]*Engineering Physics, Faculty of Natural Sciences and Technology, Saarland University, 66123 Saarbrücken, Germany, and* [∥]*Clinic of Operative Dentistry, Periodontology and Preventive Dentistry, Faculty of Medicine - Clinical Medicine, Saarland University Hospital, 66421 Homburg, Germany*

Received June 8, 2010. Revised Manuscript Received September 14, 2010

Structural and chemical changes that arise from fluoridation of hydroxyapatite ($Ca_5(PO_4)_3OH$ or "HAp"), as representing the synthetic counterpart of tooth enamel, are investigated by X-ray photoelectron spectroscopy (XPS). Elemental depth profiles with a depth resolution on the nanometer scale were determined to reveal the effect of fluoridation in neutral (pH = 6.2) and acidic agents (pH = 4.2). With respect to the chemical composition and the crystal structure, XPS depth profiling reveals different effects of the two treatments. In both cases, however, the fluoridation affects the surface only on the nanometer scale, which is in contrast to recent literature with respect to XPS analysis on dental fluoridation, where depth profiles of F extending to several micrometers were reported. In addition to the elemental depth profiles, as published in various other studies, we also present quantitative depth profiles of the compounds CaF_2, $Ca(OH)_2$, and fluorapatite (FAp) that were recently proposed by a three-layer model concerning the fluoridation of HAp in an acidic agent. The analysis of our experimental data exactly reproduces the structural order of this model, however, on a scale that differs by nearly 2 orders of magnitude from previous predictions. The results also reveal that the amount of $Ca(OH)_2$ and FAp is small compared to that of CaF_2. Therefore, it has to be asked whether such narrow $Ca(OH)_2$ and FAp layers really can act as protective layers for the enamel.

1. Introduction

The destruction of the enamel by caries is a major oral health problem in industrialized countries. In Germany, for example, the economical loss caused by caries increased from 6.4 billion euros in 2002 to 7.5 billion euros in 2004.[1] Data from clinical investigations clearly demonstrate the cariostatic effect of fluoride compounds in various forms of applications.[2−5] Although numerous experimental studies have been performed up to now,[6−9] no model comprehensively describes the reaction mechanisms of fluoride with enamel.

In principle, enamel can be affected in different ways by a F-containing agent, depending on the parameters at which the agent is applied. Fluoridation can be considered as a pure substitutional mechanism where the $(OH)^-$ groups within the crystal structure of the enamel, as mainly formed by hydroxyapatite ($Ca_5(PO_4)_3OH$ or HAp), are replaced by F^- ions, leading to the isostructural fluorapatite ($Ca_5(PO_4)_3F$ or FAp). FAp is known to be more resistant to acids than HAp and is therefore regarded to protect the tooth (for HAp and FAp, demineralization starts at pH ∼ 5.5 and pH ∼ 4.6, respectively[10]). Especially in the acidic range, fluoridation is no longer a pure substitutional mechanism and also complex chemical reactions can take place, leading to a decomposition of the initial crystal structure of the enamel by the formation of other compounds, such as, e.g., CaF_2 and $Ca(OH)_2$.[6]

The lack of understanding of the nature of fluoridation yet renders an optimization of the procedure difficult. In the present study, we investigate the chemical and structural effects of fluoridation in order to answer the following questions:

(i) How deep does fluoridation reach into the enamel layer?
(ii) Which chemical species are produced in enamel by fluoridation?
(iii) Which, if any, structural changes in the enamel take place by fluoridation?

These questions were recently dealt with by Gerth et al. using depth-selective X-ray photoelectron spectroscopy (XPS).[6] The authors proposed that, after the fluoridation by an acidic agent, the surface of enamel can be described by a three-layer-model, containing CaF_2, $Ca(OH)_2$, $Ca_5(PO_4)_3F$, and $Ca_5(PO_4)_3OH$. The results of the present work support this model, but on a completely different length scale (nanometers instead of micrometers). It is the discrepancy of the length scale that is the important result of the present study, since this questions all earlier interpretations of the effect of fluoride on enamel.

XPS is a well-established and well-suited method[11] to study the fluoridation of enamel. Combined with Ar ion etching, the surface

*Corresponding author. E-mail: f.mueller@mx.uni-saarland.de.

(1) *Gesundheit und Krankheitskosten 2002 und 2004*; Statistisches Bundesamt: Wiesbaden, Germany, 2007.
(2) A. R. Ten Cate *Oral Histology: Development, Structure, and Function*, 5th ed.; C. V. Mosby: St. Louis, MO, 1998.
(3) Ross, M.H.; Kaye, G.I.; Pawlina, W. *Histology: A Text and Atlas*, 4th ed.; Lippincott Williams & Wilkins: Philadelphia/London, 2003.
(4) Dean, H. T. *Public Health Rep.* **1938**, *53*, 1443.
(5) Dean, H. T.; Arnold, F. A.; Elvone, E. *Public Health Rep.* **1942**, *57*, 1155.
(6) Gerth, H. U. V.; Dammaschke, T.; Schäfer, E.; Züchner, H. *Dent. Mater.* **2007**, *23*, 1521.
(7) Uchtmann, H.; Duschner, H. *J. Dent. Res.* **1982**, *61*, 423.
(8) Duschner, H.; Uchtmann, H. *Caries Res.* **1988**, *22*, 65.
(9) Caslavska, V.; Duschner, H. *Caries Res.* **1991**, *25*, 27.
(10) Featherstone, J. D. B.; Ten Cate, J. M. Physicochemical aspects of fluoride-enamel interactions. In *Fluoride in Dentistry*; Ekstrand, J., Fejerskov, O., Silverstone, L.M., Eds.; Munskgaard International Publishers: Copenhagen, 1988; pp 125−149.
(11) Oechsner, H. *Thin Film and Depth Profile Analysis*; Topics in Current Physics 37; Springer: Berlin/Heidelberg/New York/Tokyo, 1984.

sensitivity of XPS allows investigating the chemistry of the surface of the sample layer-by-layer with a depth resolution in the range of 1 nm. So far, literature reports on a large variety of such investigations,[6−9] but the results of these studies are often contradictory, and therefore, there is still no consistent picture concerning the mechanism of fluoridation. In contrast, it seems that each new experiment provides new results. Especially with respect to the penetration depth of the F^- ions,[12] as representing the main indicator for fluoridation, the published data do not show a consistent dependence on the applied agent, the pH value, the fluorine concentration, or the exposure time. A possible clue to explain the discrepancies of previous studies could lie in the samples that were used to investigate fluoridation. In most of these studies,[6−9] XPS depth profiling was performed on tooth enamel (bovine or human), on powders of synthetic HAp or on nonsintered pellets of synthetic HAp, but these kinds of specimen do not represent appropriate systems to reveal the fluoridation mechanism for a single grain by a technique without spatial resolution, such as XPS, especially since the results of such experiments may be affected by structural defects and/or porosities. Therefore, the interaction between fluoride and the enamel can be deduced from these studies only with some restrictions.

On one hand, the main interest to reveal the impact of fluoride on enamel is to gain detailed insight into the mechanisms that are involved in this process in order to optimize the protection of the tooth's surface. On the other hand, the tooth itself is not necessarily an ideal model system to investigate the basic principles of fluoridation, especially since it represents a solid with a very complex (and maybe individual) structure with defects. For example, Dowker et al.[13] reported porosities of teeth up to 45%, depending on the physical condition of a particular specimen. The porosity of a tooth is expected to have a double impact on the elemental depth distributions that are finally observed in an experiment:

(1) If the agent is provided via the macroscopic surface of the sample, microporosities of the sample, especially if present as microchannels, result in a larger microscopic surface. For a particular crystallite, the agents are also provided along lateral directions, and therefore the "macroscopic" depth profile, as determined in experiment, displays a deeper penetration depth than the true depth profile for a particular crystallite.

(2) The depth profile of the F distribution is not only determined by the HAp−FAp substitution within the enamel. In addition, it can be strongly affected by an embedding of the F containing solvent within the porosities.

Both scenarios are schematically sketched in Figure 1. The surface porosity of tooth enamel is a particular problem, especially in case where the enamel crystallites are dissolved in part and exposed as a result of treatment with an acidic agent, as applied in most of the previous studies.[6−9] Since a powder can be considered as a solid with extremely high porosity, this problem is also valid for powder samples of synthetic HAp that have been also used for elemental depth profiling experiments.[6,7]

For a comprehensive understanding of the nature of fluoridation, it is therefore essential to exclude (or at least to reduce) these

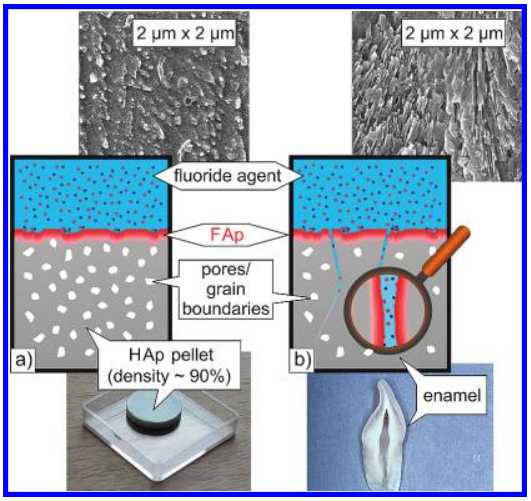

Figure 1. Schematic drawing of "fluoridation" for (a) a compact sample, as a sintered pellet of synthetic HAp with ~90% density and (b) for a porous sample, such as a tooth, HAp powder, or nonsintered HAp pellets. The compact structure of synthetic HAp and the layered, needle-like crystallite of enamel after applying an acidic agent are demonstrated by the 2 μm × 2 μm scanning electron microscope images.

porosity-related errors. Only then the depth dependence of the element composition as displayed macroscopically by the experiment is equal (or at least close) to the microscopic depth profile of each particular crystallite. For that reason, we have used sintered pellets of synthetic HAp with densities close to the crystallographic density (~90%, cf. section 2.3) to investigate the effect of fluoridation for solvents with different pH values. Although this 90%-density is comparable to the density of sound enamel,[13] there is a decisive difference between such sintered HAp samples and teeth. In contrast to the microchannels within tooth enamel, the HAp samples exhibit just a distribution of isolated pores. For the HAp samples, F is provided by just the "chemistry" of fluoridation but not by a long-range percolation of the solvent.

According to the results that are obtained for such compact samples, there is strong evidence that previous studies reporting depth-resolved elemental composition are very likely inaccurate by 1 or even 2 orders of magnitude. We assign these differences to the structural properties of the used samples, which cause the experimental depth profiles to display a superposition of fluoridation and diffusion. Depending on the contribution of diffusion, large errors can occur.

Addressing the fundamental problem of a reliable depth scaling, careful attention has also been paid to the depth calibration during Ar ion etching. Thus, in the present study, we will also describe a method developed to obtain a reliable depth scale in XPS.

2. Experimental Section

2.1. Photoelectron Spectroscopy. In XPS, slow electrons with kinetic energies in the range of a few hundred electron volts (eV) are used for probing a sample. In this range of kinetic energies, the electron mean free path within the sample is very small, resulting in an escape depth of about 1 nm.[14] Therefore, XPS provides a very high surface sensitivity for the analysis of elemental composition. It is a perfect tool to investigate elemental depth profiles, provided the sample can be ablated layer-by-layer on the nanometer scale (for details, cf. chapter 4 in ref 15).

(12) Since all intensity profiles of F can be approximated (at least roughly) by an exponential decay, we refer to the decay length as the penetration depth. For an exponential decay with amplitude A and decay length λ, the overall area of the profile is given by $A \cdot \lambda$, equal to a step-like distribution (box) of amplitude A and width λ.

(13) Dowker, S. E. P.; Elliott, J. C.; Davis, G. R.; Wilson, R. M.; Cloetens, P. *Caries Res.* **2004**, *38*, 514.

(14) Seah, M. P.; Dench, W. A. *Surf. Interface Anal.* **1979**, *1*, 2.

(15) Briggs, D.; Seah, M. P. *Practical Surface Analysis: Auger and X-ray Photoelectron Spectroscopy*, 2nd ed.; Wiley Interscience: Chichester, UK, 1990.

For a controlled ablation on the nanometer scale, Ar ion etching represents an established tool in surface science.[11,15,16] After each etching step, XPS spectra are recorded, and the characteristic core level intensities of the respective elements can be quantitatively analyzed to obtain the stoichiometry of the topmost nanometer of the sample.[11,15] It is therefore of utmost necessity to determine the etching rate with extreme care. It cannot be inferred solely from the parameters of the Ar ion source (acceleration voltage and emission current), since the actual number of Ar ions hitting the surface then remains unchecked (due to instabilities of the ion source, as, e.g., by variations of gas pressure). Instead, the number of Ar ions must be controlled directly via the measurement of the deposited charge on the sample, as shown in Appendix A.1. White light interferometry is then applied to reveal the sputter efficiency with nanometer resolution in z-scale (along the surface normal).

2.2. Experimental Setup. The experiments were performed with an ESCA Lab Mk II photoelectron spectrometer (by Vacuum Generators, Hastings, England) with an ultra high vacuum in the range of 10^{-10} mbar. The XPS spectra were recorded with Al K_α radiation ($h\nu = 1486.6$ eV) in normal emission mode (takeoff angle 0° with respect to the surface normal). The elemental composition of the samples was determined by extracting intensities from detail spectra (recorded with 20 eV pass energy) of the F-1s, O-1s, Ca-2p, Ca-2s, P-2p, P-2s, Na-1s (NaF agent), and N-1s (Olaflur agent) core levels. The spectra were normalized to the photon flux and the corresponding orbital specific photoemission cross section, as listed in ref 17. For Ca and P, the stoichiometry was averaged by the values derived from the 2p and 2s core level intensities. Due to the insulating nature of HAp, the samples exhibit a strong charging (~15 eV) that was not compensated by applying charge neutralization (as, e.g., by using a flood gun). For the calibration of the binding energies, it was not possible to refer to the C-1s binding energy because the C-1s intensity strongly drops with increasing depth. Instead, the binding energy of the P-2p electrons was used as a reference, because in the structural models, as discussed below, P is only contained in HAp and FAp. In these compounds, the P-2p energies just differ by 200 meV (HAp: 133.8 eV,[18] FAp: 133.6 eV,[18] mean value 133.7 eV as P-2p reference). The Ar ion etching was performed with a IQ-100 ion source (by Vacuum Science Instruments, Bad Schwalbach, Germany) with an acceleration voltage of 4 keV and an emission current 10 mA, resulting in an Ar ion current of ~1 μA at the sample and an etching rate of ~0.12 nm/min. For details of the calibration of the Ar ion etching, see Appendix A.1; for details of the XPS technique, see ref 19.

2.3. Preparation of the Samples. The preparation of the HAp pellets began with several cycles of filtration of a commercial HAp powder (by Fluka/Sigma Aldrich, Taufkirchen, Germany) in order to remove impurities such as sodium and chlorine. The structural quality of the HAp powder was checked by X-ray diffraction (XRD), which exactly displays the diffraction pattern[20] of the hexagonal $P63/m$ space group (cf. Figure 2). The powder (~1 g) was pressed (~8 tons/cm^2) to pellets (Ø ~ 16 mm, h ~ 2.5 mm) with green densities of 60−65% (HAp: $\rho = 3.156$ g/cm^3), followed by sintering at about 1150 °C using the temperature profile given in ref 21. This procedure finally results in a density (as given by the mass-to-volume ratio of a cylindrical pellet) that is 90% of the theoretical value (as given by the atomic mass-to-volume ratio of a crystallographic unit cell).

With respect to the chemical composition of the sintered HAp samples, the XPS data provide a stoichiometry of Ca:O:P = 5:12.7:3.1, which is very close to the nominal 5:13:3 ratio of the $Ca_5(PO_4)_3OH$ compound (note that the H content cannot be detected in XPS).

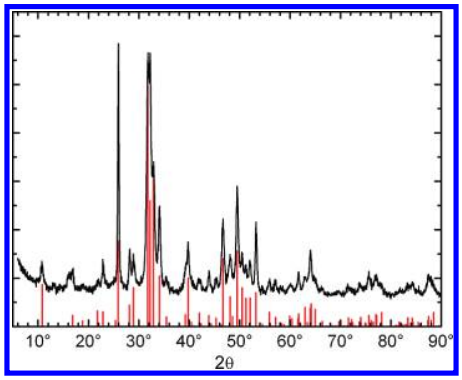

Figure 2. XRD data of an untreated HAp powder (black line), compared to the diffraction pattern of the $P63/m$ space group (red bars), as taken from ref 20.

For fluoridation, the HAp pellets were exposed to a NaF agent (246 ppm, by Gaba, Basel, Switzerland) and an Olaflur agent (242 ppm, by Gaba) with pH = 6.2 and 4.2, respectively, at 37.5(5) °C for 5 min. After fluoridation, the samples were transferred to the vacuum system in the "wet state", and residues of the agent were removed by evacuating the entrance lock of the vacuum system down to 10^{-5}−10^{-6} mbar. After fluoridation, an additional rinsing of the samples by, e.g., distilled water, was not applied in order to avoid an ablation of any physisorbed species that are formed after or during the application of the agent.

3. Results

Fluoridation of HAp in the nearly neutral NaF agent and in the acidic Olaflur agent results in strong differences in the elemental depth profiles of the sample. After the NaF treatment, the depth profiles display the characteristics of a HAp−FAp substitution mechanism, while the depth profiles after the Olaflur treatment indicate strong structural and chemical modifications of the sample.

3.1. NaF Agent (246 ppm, pH = 6.2). For the sample exposed to the NaF agent (246 ppm, pH = 6.2, 5 min at 37 °C), the XPS intensities (scaled as relative number of atoms) for O (Figure 3a), Ca (Figure 3c), and P (Figure 3d) can be approximated by nearly constant values that display the elemental composition of the untreated HAp sample. Hence, the nearly neutral NaF solvent does not affect the initial Ca:P:O ratio. The step-like distribution for C (as representing an unavoidable, but nonrelevant impurity) in Figure 3b gives evidence that all ex situ effects, such as, e.g., by adsorbates or impurities of the agent, are removed after 2−3 steps of preparation (corresponding to a thickness of about 1 nm).

In contrast to Ca, O, and P, the intensity distribution of F in Figure 3e shows noticeable depth dependence that can be approximated by an exponential decay with a decay length of about 6 nm and an amplitude of about 4% of the total oxygen amount, corresponding to about 50% of the $(OH)^-$ groups. Since this 4% effect is smaller than the scattering of the data for oxygen in Figure 3a, the substitution of $(OH)^-$ groups by F^- ions is not displayed in the oxygen intensity in Figure 3a.

In Figure 3f, a distinct Na intensity can also be observed, probably caused by the absorption of NaF agent (see section 4.1). Similar to the F distribution in Figure 3e, the Na distribution also shows an exponential decay, but with smaller decay length (~ 1.6 nm) and smaller amplitude (~ 40% of F amplitude), resulting in a Na:F ratio of about 0.1, much smaller than the 1:1 ratio

(16) Carter, G.; Vishnyakov, V. *Surf. Interface Anal.* **1995**, *23*, 514.
(17) Yeh, J. J.; Lindau, I. *At. Data Nucl. Data Tables* **1985**, *32*, 1.
(18) Landis, W. J.; Martin, J. R. *J. Vac. Sci. Technol. A2* **1984**, 1108. P-2p: 133.8 eV (HAp), 133.6 eV (FAp); Ca-2p$_{3/2}$: 347.8 eV (HAp), 347.6 eV (FAp); F-1s: 684.6 eV (FAp) .
(19) S. Hüfner, *Photoelectron Spectroscopy, Principles and Applications*, 3rd ed.; Springer: Berlin/Heidelberg/New York, 2003.
(20) Entry 74−565 of database Powder Diffraction File PDF 2, Release 2001, International Centre for Diffraction Data (ICDD), Newtown Square, PA, USA.
(21) Prokopiev, O.; Sevostianov, I.; Genin, J.; Munson McGee, S.; Woodward, C. *Int. J. Fract.* **2004**, *130*, L183.

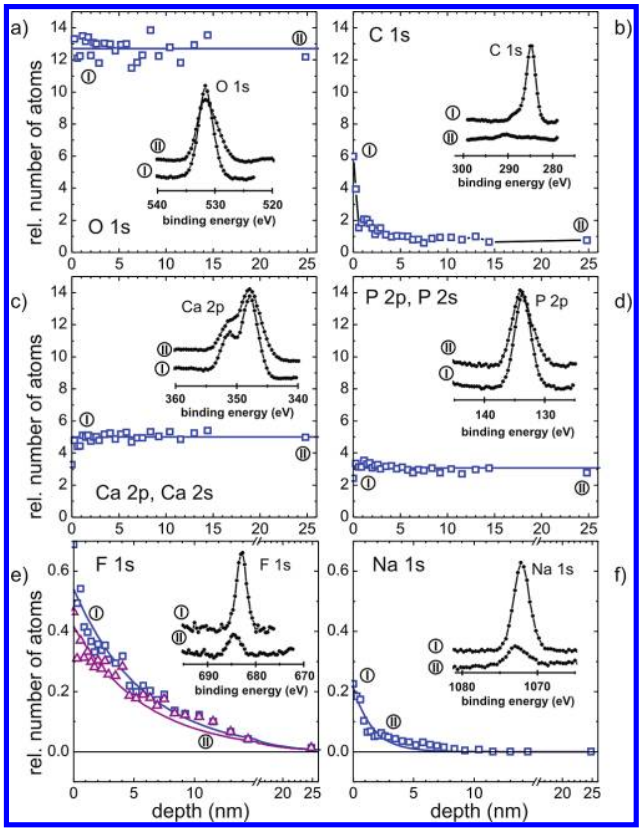

Figure 3. XPS depth profiling (atomic ratios) of a synthetic HAp sample after 5 min of fluoridation in NaF (246 ppm, pH = 6.2, 37.5(5) °C): (a) oxygen, (b) carbon, (c) calcium, (d) phosphorus, (e) fluorine, (f) sodium (note the different abscissa for F and Na compared to (a)-(d)). The insets show the detailed spectra that have been used to calculate the XPS intensities (for Ca and P, only the 2p spectra are shown).

of the NaF solvent. If the F distribution is rescaled by the Na distribution (cf. triangles in Figure 3e), the amplitude of the F intensity is slightly reduced to about 40% of the $(OH)^-$ groups while the decay length remains unchanged in the range of about 6 nm.

In Figure 4a, the Ca-2$p_{3/2}$ binding energy (blue dots) shows no depth dependence, and it is distributed around the value characteristic for apatite (FAp or HAp,[18] black line). In contrast to Ca-2$p_{3/2}$, the F-1s binding energy in Figure 4b (blue dots) starts at lower values, as characteristic for NaF,[22] and with increasing depth, it approaches the value characteristic for FAp.[18]

These data give evidence that the application of the nearly neutral NaF agent results in two mechanisms: first, a fluoridation of the HAp sample by replacing a part of the $(OH)^-$groups by F^- ions, and second, to a much lower extent, an absorption of NaF species from the agent. At this stage, it is important to point out that the decay length of the F^- ions of about 6 nm is much smaller than the values hitherto reported in literature.[6−9] We attribute this strong difference to the fact that for our compact samples, the absorption of the NaF agent just plays a secondary role (for details, cf. section 4).

3.2. Olaflur Agent (242 ppm, pH = 4.2). For the sample exposed to the Olaflur agent (242 ppm, pH = 4.2, 5 min at 37.5(5) °C, red data), Figure 5 displays considerable differences in the depth profiles for all elements, as compared to the previous sample (for comparison, the gray data represent the results for the NaF-treated sample from Figure 3).

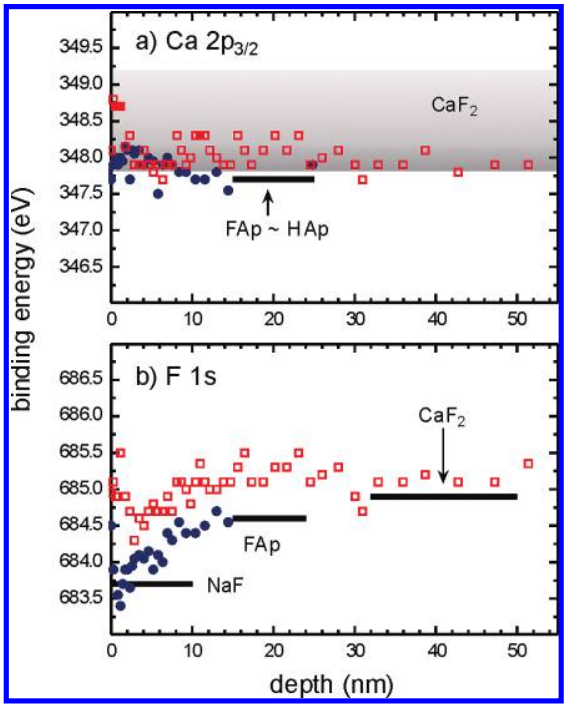

Figure 4. Depth dependence of binding energies for (a) Ca-2$p_{3/2}$ and (b) F-1s after application of NaF agent at pH = 6.2 (blue dots) and Olaflur agent at pH = 4.2 (red squares). The binding energies are calibrated to the P-2p energy at binding energy at 133.7 eV (mean value of HAp at 133.8 eV and FAp at 133.6 eV[18]). For Ca-2$p_{3/2}$ in panel a, the shaded area refers to the binding energy range for CaF_2,[23−25] and the black line refers to the binding energy for HAp/FAp.[18] For F-1s in panel b, the black lines refer to binding energies for NaF,[22] FAp,[18] and CaF_2.[25]

The most prominent change is seen in the F distribution in Figure 5e. The F^- ions obviously range much deeper into the sample (far beyond the range measured here) with a decay length of about 80 nm (cf. 6 nm for NaF). In addition, the initial F intensity has increased by more than 1 order of magnitude compared to the value for the NaF-treated sample (note the axis break of the abscissa in Figure 5e).

In contrast to the NaF agent, the application of the acidic Olaflur agent also changes the P, Ca, and O concentrations considerably. In Figures 5a and 5c, the O and P distributions start with smaller values and smoothly approach the values of the NaF-treated sample (which also represent the values of an untreated sample). For Ca, the situation is reversed in Figure 5c, i.e., the Ca distribution approaches the values of the NaF treated sample by starting at slightly increased values. These different distributions of Ca, O, and P demonstrate a considerable change in the chemistry of the HAp sample, and it must be expected that the interaction between the acidic agent and the HAp sample results in a decomposition of the HAp structure, probably to more volatile species.

Similar to that in the NaF-treated sample, the C distribution exhibits a step-like shape in Figure 5b, i.e., again, ex situ effects are removed after 2−3 etching cycles (∼1 nm). In Figure 5f, the N intensity at the surface is about 5% of the initial F intensity, and it

(22) Morgan, W. E.; Van Wazer, J. R.; Stec, W. J. *J. Am. Chem. Soc.* **1973**, *95*, 751. F-1s: 683.7 eV (NaF) .

(23) Wagner, C. D. *Handbook of X-Ray and Ultraviolet Photoelectron Spectroscopy*; Briggs, D., Ed.; Heyden: London, 1977; Chapter 7. Ca-2$p_{3/2}$: 347.9 eV (CaF_2).

(24) Seyama, H.; Soma, M. *J. Chem. Soc. Faraday Trans.* **1984**, *80*, 237. Ca-2$p_{3/2}$: 349.2 eV (CaF_2) .

(25) Nefedov, V. I.; Salyn, Y. V.; Leonhardt, G.; Scheibe, R. *J. Electron Spectrosc. Relat. Phenom.* **1977**, *10*, 121. Ca-2$p_{3/2}$: 347.8 eV (CaF_2); F-1s: 684.8 eV (CaF_2) .

decreases to zero with a decay length of about 0.3 nm. Therefore, it can be expected that only negligible amounts of the Olaflur agent are adsorbed at the surface, which are removed (similar to C) by just 1−2 etching cycles, i.e., a diffusion of the agent into the sample can be excluded.

With respect to the binding energies, the situation is also different compared to the NaF treated sample. The Ca-2$p_{3/2}$ binding energy in Figure 4a (red squares) as well as the F-1s binding energy in Figure 4b (red squares) are slightly increased and they can be assigned to the formation of CaF_2,[23−25] i.e., to that compound that represents the main contribution in the models discussed below.

According to these data, the acidic Olaflur agent is expected to result in a different fluoridation mechanism that is accompanied by a modification of the crystal structure in the surface region.

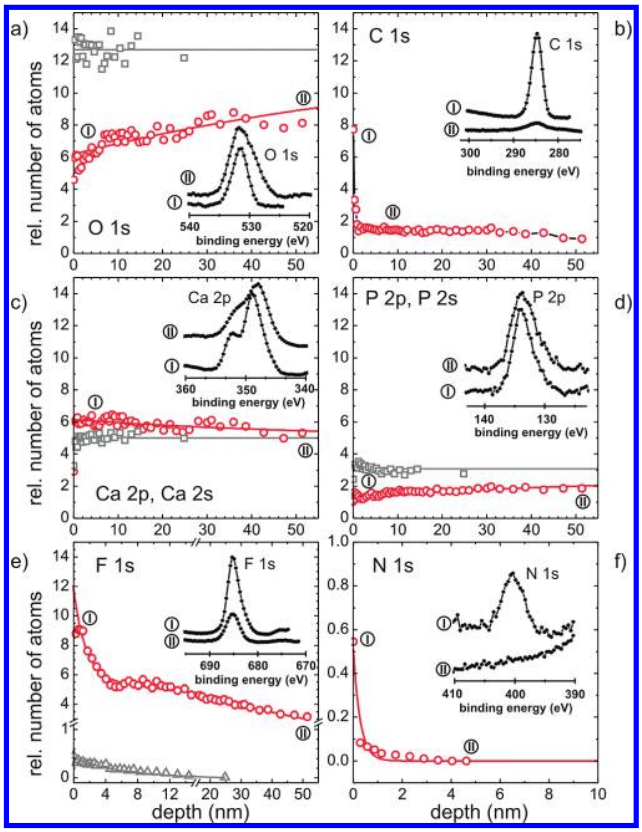

Figure 5. XPS depth profiling (atomic ratios) of a synthetic HAp sample after 5 min of fluoridation in in OlaFlur (242 ppm, pH = 4.2, 37.5(5) °C, red circles): (a) oxygen, (b) carbon, (c) calcium, (d) phosphorus, (e) fluorine, (f) nitrogen. For comparison, the data for the NaF agent from Figure 3 are also shown (gray squares). The insets show the detailed spectra that have been used to calculate the XPS intensities (for Ca and P, only the 2p spectra are shown).

4. Discussion

Before discussing our results in detail, we first refer to the results of previous studies. Although fluoridation of enamel (or synthetic HAp) was investigated in a large variety of XPS depth profiling experiments,[6−9] it is difficult to compare the results of these studies, especially since the experimental parameters, such as specimen (bovine or human enamel, synthetic HAp as powder or as pellets), applied agent, pH value, fluorine concentration, and exposition time, are spread over a wide range, as outlined in Table 1. Especially with respect to the depth distribution of the F^- ions, the data in Table 1 do not exhibit a systematic dependence on these parameters. For example, for a short-term (1 min) fluoridation of human enamel in an acidic 250 ppm agent (pH = 4), Gerth et al.[6] observed a large depth distribution of about 4.5 μm, while in the present study, the fluoridation of a synthetic HAp sample using identical parameters leads to a depth distribution that is about 60 times smaller, namely, 77 nm, although the exposition time was extended to 5 min. For fluoridation of bovine incisors, the depth distribution reported by Duschner[8] and by Caslavska[9] differ only by a factor 2 (750 and 325 nm, respectively), although the exposure times as well as the concentrations and the pH values of the applied NaF agents were strongly different. These two examples suggest that a comparison of data obtained by different authors is difficult and needs to be revised.

However, in all studies that include a systematic variation of the pH value,[8,9] an extended depth profile of F was observed with decreasing pH value, concurrent with a depletion of phosphorus content. More precisely, after fluoridation at low pH values, the phosphorus content at the surface of the sample is lower than that of an untreated sample, whereby the affected depth range of P depletion is similar to that of the F decrease. It is known that these phenomena indicate a structural change by acidic agents, which may result in less mechanical and chemical stability of the enamel surface.

4.1. NaF Agent (246 ppm, pH = 6.2). According to the intensity profiles in Figure 3, the application of the nearly neutral

Table 1. Comparison of Experimental Parameters for Fluoridation and Decay Lengths for F^- Depth Profile Ranges As Published by Various XPS Studies

sample[a]	agent[b]	pH	concent.	treatment	decay length[c] (nm)	ref.
HAp	NaF	6.2	250 ppm	5 min 37 °C	6	this work
BEn	NaF	6.0	1000 ppm	10 min 37 °C	9 (S)[d] 191 (B)[d]	9
BEn	NaF	6.0	30 ppm	10 min 37 °C	325[d]	9
BEn	NH_4F	6.0	1000 ppm	10 min 37 °C	46 [d]	9
BEn, HAp	NaF	5.5	~ 22000 ppm (2.3 wt % F)	30 min 35 °C	12 (S) 60 (B)	7
BEn	NaF	5.0	~ 950 ppm (0.1 wt % F)	30 min 37 °C	720 [d]	8
BEn	amine hydrofluoride	5.0	0.1 wt % F	30 min 37 °C	550 [d]	8
HAp	OlaFlur	4.2	250 ppm	5 min 38 °C	1.5 (S) 77 (B)	this work
BEn	NaF	4.0	~ 950 ppm (0.1 wt % F)	30 min 37 °C	750 [d]	8
BEn	amine hydrofluoride	4.0	0.1 wt % F	30 min 37 °C	1130 [d]	8
BEn	NH_4F	4.0	1000 ppm	10 min 37 °C	910 [d]	9
HEn	OlaFlur	4.0	250 ppm	1 min 20 °C	4500	6

[a] HAp: synthetic hydroxyapatite, BEn: bovine enamel, HEn: human enamel. [b] For a detailed description of the agent, the reader may consult the references. [c] Some depth profiles cannot be approximated by a single exponential decay. In these cases, (B) and (S) refer to bulk and surface contributions. [d] Extracted from the F intensity ratios for treated and untreated samples.

NaF solution to the HAp sample has no noticeable impact on the elemental distribution of O, Ca, and P. Therefore, it can be expected that the absorption of F^- ions by the HAp sample indeed results in a fluoridation mechanism in terms of a pure substitution of the $(OH)^-$ groups by F^- ions from the agent, leading to the formation of the isostructural FAp compound. This picture is also supported by the Ca-$2p_{3/2}$ binding energy in Figure 4a (blue), indicating (at least roughly) that Ca is only present as apatite. With respect to the parameters for the exponential intensity distribution of F in Figure 3e, the HAp−FAp transformation starts by replacing 40% of the $(OH)^-$ groups by F^- ions, and it decreases with a decay length of about 6 nm.

This decay length is much smaller (up to 1 to 2 orders of magnitude) than the values reported in previous studies (see Table 1) and one has to critically ask where these deviations come from. This question is answered (at least indirectly) by the observation of very small Na intensities in Figure 3f. Comparing the total amount of F and Na in Figure 3e,f, the Na:F ratio corresponds only to 10% of the Na:F = 1:1 ratio of the agent. Therefore, it can be expected that after the fluoridation of the HAp sample by the NaF agent, the overall F distribution in Figure 3e displays two different mechanisms: the fluoridation of the HAp sample as well as the absorption of NaF species from the agent within the pores or grain boundaries of the sample. However, due to the very small overall amount of Na, the latter process seems to plays a secondary role. With respect to the large differences in the decay lengths of F, we assume that in some of the previous studies the situation is reversed, i.e., the observed F distribution displays the absorption of Na^+ and F^- species from the agent rather than the fluoridation of the HAp crystallites. In our experiment, the NaF agent was applied to a HAp sample with a density of about 90%, and the small portion of isolated pores strongly suppresses diffusion of the agent into the sample. Therefore, the absorption of Na is expected to be restricted to a small range near the surface, as experimentally confirmed by the small decay length of the Na intensity (∼1.6 nm) in Figure 3f. Hence, the observed F distribution in Figure 3e mainly displays the fluoridation of the sample via the uptake of F^- ions during the HAp−FAp transformation. In order to support this assumption, we refer to the study of Uchtmann et al.[7] that reports a Na:F ratio of 1:1 for depths up to 300 nm (and beyond) after the fluoridation of synthetic HAp by a NaF agent (cf. Figure 9 in ref 7). Compared to our values from Figure 3e,f, these depths differ by nearly 2 orders of magnitude, and we attribute this strong difference to the different microstructures of the HAp samples. In ref 7, synthetic HAp powder was pressed by 6000 kp/cm^2 (∼6 tons/cm^2), which is close to the pressure applied in the present study (8 tons/cm^2). However, since the authors give no information on additional sintering, their HAp samples are expected to exhibit densities similar to the green densities of our HAp samples before sintering, i.e., densities in the range of 60%. For such a specimen, the large amount of pores then favors a percolation of the agent, resulting in a depth distribution of F that displays the absorption of the NaF agent rather than the fluoridation of the crystallites. This scenario would be also in accordance with the observation of two different decay lengths for the F distributions in ref 7 (see also Table 1). The small decay length probably displays the absorption of F^- ions by fluoridation (with the value of 12 nm being comparable to our value of 6 nm) while the larger decay length of about 60 nm then displays F contributions due to the absorption of the agent.

According to the data in Figure 3e, the application of the NaF agent at pH = 6.2 leads to the result that the F^- ions penetrate the sample with a decay length of only about 6 nm. This provides an interesting result for two reasons:

First, this small value (or at least its order of magnitude) seems to be confirmed by a molecular dynamic simulation by de Leeuw[26] concerning the F−HAp interaction. In this study, the calculations predict that F^- replaces $(OH)^-$ mainly within the topmost layers of the HAp sample, and no considerable penetration into the bulk is expected. In addition to a partial F^-−$(OH)^-$ substitution, i.e., FAp/HAp formation by incorporation of F in the HAp lattice, also an adsorption of F on the HAp surface might be expected, i.e., f-HAp formation.[27]

Second, a decay length of about 6 nm is close to the daily wear of human teeth (∼3 nm per day, assuming an annual wear of human enamel of about 1 μm[28]). Therefore, a daily application of nearly neutral NaF agent would result in a fluoridation of exactly that part of the tooth that is ablated between two applications. At first sight, this looks as an optimal procedure, but on the other hand, one has to critically ask whether a 6 nm FAp layer indeed acts as a protective layer. This question will be investigated in detail in a subsequent study.

4.2. Olaflur Agent (242 ppm, pH = 4.2). In contrast to the application of the nearly neutral NaF agent that just results in a fluoridation in terms of a HAp−FAp transition by replacing the $(OH)^-$ groups by F^- ions, the application of the acidic Olaflur agent (pH = 4.2) also considerably changes the observed P, Ca, and O distributions in Figure 5. Therefore, an additional decomposition of the HAp structure has to be expected. This phenomenon has also been observed in previous studies that report a change in the surface structure to an ablation depth up to several micrometers,[6,7,9] and especially the recent study by Gerth et al.[6] has given detailed insight into such structural modifications. For the fluoridation by an acidic agent, the authors proposed a three-layer model whereby the fluoridated enamel is formed by a stacking (from outside to inside) of CaF_2, $Ca(OH)_2$, $Ca_5(PO_4)_3F$, and $Ca_5(PO_4)_3(OH)$. For these compounds, depth profiles have been presented based on an analysis of the depth dependence of the chemical shifts for the Ca-$2p_{3/2}$ binding energy.[6]

In this study, we present a different method to extract depth profiles for CaF_2, $Ca(OH)_2$, $Ca_5(PO_4)_3F$, and $Ca_5(PO_4)_3(OH)$ from XPS data. Apart from an analysis of binding energies, it is also possible to refer to the elemental depth profiles of the Ca, O, P and F intensities (as given in Figure 5) to obtain the depth profiles of the compounds.[29]

In order to give quantitative depth profiles for the CaF_2, $Ca(OH)_2$, $Ca_5(PO_4)_3F$, and $Ca_5(PO_4)_3(OH)$ compounds, the elemental depth profiles in Figure 5 were approximated by exponential decay/growth, as shown in Figure 6a. Here, we took as a constraint that the limiting values for Ca, O, and P are given by the values of the NaF data in Figure 3, which also represent the values for an untreated sample due to the small overall content of F. From the elemental depth profiles, it is then straightforward (for details, see Appendix A.2) to extract the depth profiles of the compounds, as depicted in Figure 6b for CaF_2 and $Ca(OH)_2$ and Figure 6c for $Ca_5(PO_4)_3F$ and $Ca_5(PO_4)_3(OH)$. Although the calculation of the depth profiles was not restricted by a required order of these compounds, our result displays the configurational order that was proposed by Gerth et al.,[6] i.e., the surface region is mainly formed by CaF_2, followed by $Ca(OH)_2$ and the HAp and

(26) de Leeuw, N. H. *J. Am. Chem. Soc. B* **2004**, *108*, 1809.
(27) Gasser, P.; Vogel, J. C.; Gramain, P. *J. Colloid Interface Sci.* **1994**, *168*, 465.
(28) Joiner, A.; Philpotts, C. J.; Cox, T. F.; Schwarz, A.; Huber, K.; Hannig, M. *J. Dent.* **2008**, *36*, 360.
(29) In XPS, an analysis of binding energies is always a difficult task as soon as the sample exhibits poor conductivity (as apatite) and charging effects take place. In contrast, a not well-defined binding energy axis has no impact on the overall intensity distribution, and therefore an analysis of intensity distributions can be applied even for setups with no facilities for charge compensation.

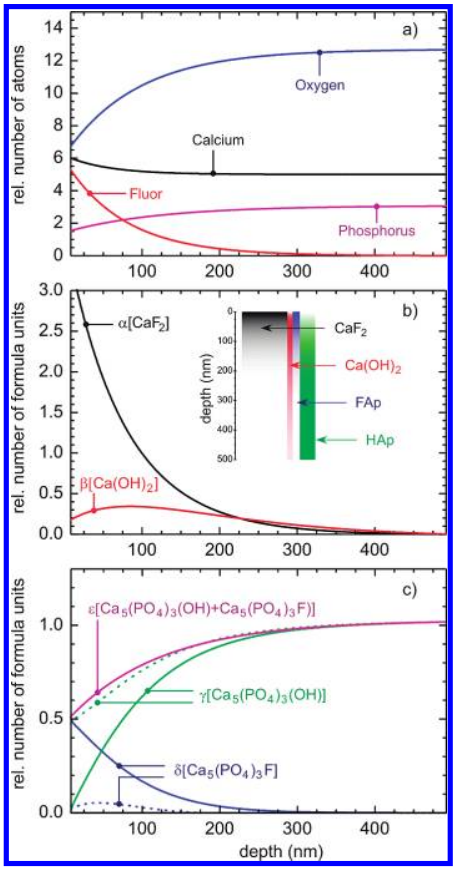

Figure 6. (a) Approximation of the elemental depth profiles from Figure 5 as an exponential decay/growth. (b) Depth profiles of the calcium compounds CaF_2 and $Ca(OH)_2$, as calculated by the elemental distributions from panel a, according to the procedure listed in Appendix A.2 (for α and β, see Appendix). (c) Depth profiles of the apatites FAP and HAp, as calculated by the elemental distributions from panel a, according to the procedure listed in Appendix A.2 (for $\gamma-\varepsilon$, see Appendix). The solid (dashed) lines for the HAp and FAp disributions represent the case of maximal (minimal) FAp content (for explanation, see Appendix A.2). The inset in panel b gives a schematic drawing of the depth profiles for the compounds for the case of maximal FAp content. The saturation of the color represents the relative depth distribution of each compound, and the width of each color bar represents the maximal relative amount of each compound.

FAp apatites. In addition, it is also amazing that the shapes of the depth profiles for the compounds in Figure 6b,c, as based on our analysis of elemental intensity distributions, are very similar to those given by Gerth et al.,[6] as based on an analysis of binding energies. However, the results of the intensity analysis show that the stoichiometry of the CaF_2 "layer" has to be rescaled to $CaF_{1.43}-CaF_{1.57}$ in order to avoid nonphysical intensity distributions (cf. Appendix A.2).

Therefore, the proposed three-layer model[6] seems to be qualitatively supported by the present results, but on a completely different length scale. In addition, the term "layer" seems to be unfavorable, because the profiles in Figure 6b,c give evidence that these "layers" exhibit strong intercalation instead of forming sharp interfaces (therefore, no distinction between FAp, HAp, FHAp, and f-HAp is made). Within this context, the results in Figure 6b,c also show that the FAp and $Ca(OH)_2$ "layers" provide only a small overall contribution after the surface modification by the fluoride, compared to the large amount of CaF_2. In general, the fluoridated sample is mainly formed by CaF_2 and HAp, where CaF_2 switches to HAp at a depth of about 125 nm. This value is in accordance to the results reported by Petzold in ref 30, where a similar treatment of the sample (60 s at pH = 4.5) results in the formation of CaF_2-like spheres with diameters ranging from 120 to 300 nm.

At least from the chemical point of view, the presence of $Ca(OH)_2$ is a crucial point because this compound is expected to dissolve in the acidic solution. Together with the observation of an enrichment of Ca at the surface, i.e., $CaF_{1.43}-CaF_{1.57}$ instead of CaF_2, the results of our intensity analysis in Appendix A.2 can also be interpreted in terms of the model given by Petzold.[30] In ref 30, the "CaF_2-like" material contains additional amounts of O and P within the CaF_2 spheres with P and O contribution strongly depending on the application time of the solvent. For short-term treatment (with parameters close to our values) there is only additional amount of O within the CaF_2 spheres, and contributions from P can be neglected, resulting in a Ca:F ratio of 1:1.23. This ratio is closer to our $CaF_{1.43}-CaF_{1.57}$ stoichiometry than to the regular CaF_2 stoichiometry used by Gerth et al.[6] Therefore, the intensity distribution of $Ca(OH)_2$ may display the contribution of additional O within the CaF_2 spheres rather than the presence of real "$Ca(OH)_2$" (note that H is not detectable by XPS). This seems to also be supported in Figure 6b by the "CaF_2" and "$Ca(OH)_2$" distributions that share a common range. Consequently, the results of our analysis of XPS intensities data are not in contrast to the XPS data by Gerth et al.,[6] but because of the large differences in the ablation depths and due to the observation of nonstoichiometric $CaF_{x<2}$, our data seem to rather support the atomic force micrscopy/energy dispersive X-ray spectroscopy (AFM/EDX) study by Petzold.[30]

A further modification of the three-layer model by replacing $Ca(OH)_2$ by calcium carbonate can be excluded because, for the Olaflur-treated sample, the amount of carbon in Figure 5b is the same as that in Figure 3b for the NaF-treated sample and must be assigned to ubiquitous contaminations.

With respect to the modification of crystal structure, the XPS data in Figures 5 and 6 are in accordance with the results of previous XPS studies,[6−9] but similar to the case of the NaF agent, there are strong differences concerning the depth scale, and again, one has to refer to the effect of porosity to explain such discrepancies.

The XPS data of the present study also fit well with the AFM observations reported by Petzold,[30] especially with regard to the depth scale of fluoridation and chemical modification of the HAp surface with a high amount of CaF_2 after application of an acidic amine fluoride solution for 5 min. In these AFM investigations[30] it is shown that the enamel surface is covered by a continuous layer of spherical CaF_2 globules (diameter of 120−300 nm) within minutes after the treatment with 0.1% amine fluoride (pH = 4.5), whereas a treatment with a neutral NaF solution caused the formation of only a few scattered CaF_2 globules. These findings indicate that the fluoride deposition in form of CaF_2 precipitates is affected by the pH value of the fluoride containing solution. The accelerated dissolution of the enamel apatite at lower pH provides more free calcium ions, and, thus, it favors the precipitation of the CaF_2 globules.

Irrespective of the "right" depth scale, i.e., irrespective of whether the F^- ions penetrate into the enamel up to 77 nm (our value from Figure 5e) or up to several micrometers (literature values, cf. Table 1), the results also show that just one application of an acidic agent results in a penetration depth that approximately amounts to more than the monthly (from our values) or

(30) Petzold, M. *Caries Res.* **2001**, *35*, 45.

yearly (from literature values) wear of a tooth, thus influencing the surface of the tooth considerably.

5. Conclusion

With respect to the application of the acidic Olaflur agent at pH = 4.2, the data of the present study are not in contradiction to the three-layer $CaF_2-Ca(OH)_2-FAp/HAp$ model by Gerth et al.[6] However, the quantitative analysis of the data shows that the $Ca(OH)_2$ and FAp (even if its amount is assumed to be maximal, see Appendix A.2) contributions only play a secondary role. The surface area is mainly dominated by large amounts of CaF_2, and, as a consequence, such a surface may be less stable than the original one containing HAp. Due to the fluoridation at pH = 4.2, an extended "layer" of caries-protecting F^- ions is achieved, but according to Figure 6 as CaF_2 rather than as a protecting FAp layer. According to the AFM study by Petzold, CaF_2 is distributed as a layer of densely packed spheres with diameters ranging from 120 to 300 nm.[30]

Since the F ions have only a small penetration depth, F ions have to be continuously administered (as, e.g., by the regular use of a neutral fluoridated toothpaste or mouthrinse) since the protecting FAp layer is only as thick as the daily wear of enamel.[28]

In principle, fluoride can induce cariostatic effects by (1) reducing enamel solubility when incorporated into the mineral structure; (2) by fostering the remineralization of incipient enamel lesions and the deposition of fluoridated phases (within dental plaque), which provide a source of mineral ions (Ca, P, F) under acidic conditions; and (3) by reducing the net rate of transport of matter out of the enamel surface, under acidic conditions, by inducing the reprecipitation of fluoridated HAp phases within enamel. On the basis of an analysis of clinical and laboratory data, it was already concluded two decades ago by Margolis and Moreno[31] that the benefits provided by fluoridation result, to a large degree, from topical effects. Thus, clinical procedures are recommended that establish and maintain low levels of free fluoride in plaque fluid.[32] This will require frequent exposure to topical fluorides.[31]

6. Summary

The results of the present study on the fluoridation of synthetic HAp samples qualitatively match the results reported in literature. First, the fluoridation by a nearly neutral agent leads to a substitution of the $(OH)^-$ group by the F^- ions with no changes in the chemistry and structure of the initial compound, i.e., a partial transition from HAp to the isostructural FAp takes place (FHAp). Second, the fluoridation by an acidic agent results in considerable changes in the surface structure of HAp by the formation of other compounds, such as $Ca(OH)_2$, FAp, and CaF_2, as previously proposed by Gerth et al.[6] or by the formation of a "CaF_2 material", i.e., CaF_2 with additional P and O included, as proposed by Petzold.[30] Qualitatively, the results of the present study are not in contrast to the three-layer model from Gerth et al.,[6] but the suggested contribution of $Ca(OH)_2$ could also display the O impurities within the CaF_2 spheres, as observed by Petzold in ref 30. The latter model seems to be favored by the results of the present study since the presence of a "CaF_2-like" material on the HAp surface ($CaF_{1.43-1.57}$) as well as the same depth scale for the distribution of this material is observed.

(31) Margolis, H. C.; Moreno, E. C. *J. Dent. Res.* **1990**, *69*, 606.
(32) Fejerskov, O. *Fluorides in Dentistry*; Munksgaard International Publishers: Copenhagen, 1994.

However, quantitatively, the results of the present investigation are in contrast to previous XPS studies: First, the depth profiles of F are extended in a considerably lower range (1−2 orders of magnitude!) compared to the range reported by other authors, although the fluoridation was performed under similar conditions (cf. Table 1). We attribute these large deviations in depth profiles to the different microstructure of the samples. In principle, the depth profiles, as displayed by a macroscopic sample, must be regarded as a superposition of fluoridation of single crystallites and diffusion of the agent into the pores of the sample. In the case of a synthetic HAp pellet with a density of about 90%, as used in the present study, the latter process is strongly suppressed and the depth profiles, as displayed by the macroscopic sample, are close to the depth profiles of the single crystallites. For teeth (and also for HAp powders or not sintered HAp pellets), the impact of diffusion depends on the porosity of the actual sample, and therefore the depth profiles of the macroscopically probed samples can display the diffusion rather than the fluoridation of the single crystallites, as observed by the large ablation depths for F (and also Na) in previous studies.[6−9]

However, in the case of a nearly neutral agent, our low values of the penetration depth are in accordance with dynamical simulations,[26] while in the case of the acidic agent, our values are in accordance with AFM data.[30]

Finally, one has to ask of the protective power of such ultrathin FAp layers: Is it possible to save your dentition by "the skin of your teeth"? This question will be addressed in a future study.

Acknowledgment. This work was partly supported by the Deutsche Forschungsgemeinschaft within the Collaborative Research Centre 277 "Grenzflächenbestimmte Materialien", the Priority Programme SPP 1164 "Nano- & Microfluidics", and by Saarland Ministry of Finances special research funds. The authors thank H. P. Beck, R. Haberkorn, H. Kohlmann, U. Hartmann, and A. English for providing their facilities and know-how for the preparation of the HAp pellets.

Appendix

A.1. Calibration of the Ar Ion Etching Dose. The information needed for a precise depth calibration is the sputter efficiency (etching rate). Therefore, the achieved etching depth has to be measured as a function of deposited Ar ion dose on the sample. The latter can be quantified by measuring the (time-integrated) current that flows off the sample, while the resulting etching depth can be determined by white light interferometry (in this study, a New View 200 3D Imaging Surface Structure Analyzer by Zygo Corporation, Middlefield, CT, was used).

Figure 7 depicts a schematic drawing of the setup as used for the calibration of the etching rate. Figure 7a shows the setup of the HAp sample as used during the depth profiling experiments. The HAp sample is covered by a metallic ring that acts as an Ar ion collector, i.e., the Ar ion current (a few microamperes) that flows off this metallic ring is an instantaneous real-time measure for the relative number of Ar ions that hit the sample within each particular period of time:

$$I(Ar^+) \sim \frac{dn^+}{dt}$$

Since the rate of Ar ion deposition is also a direct measure of the etching rate

$$\frac{dz}{dt} \sim \frac{dn^+}{dt}$$

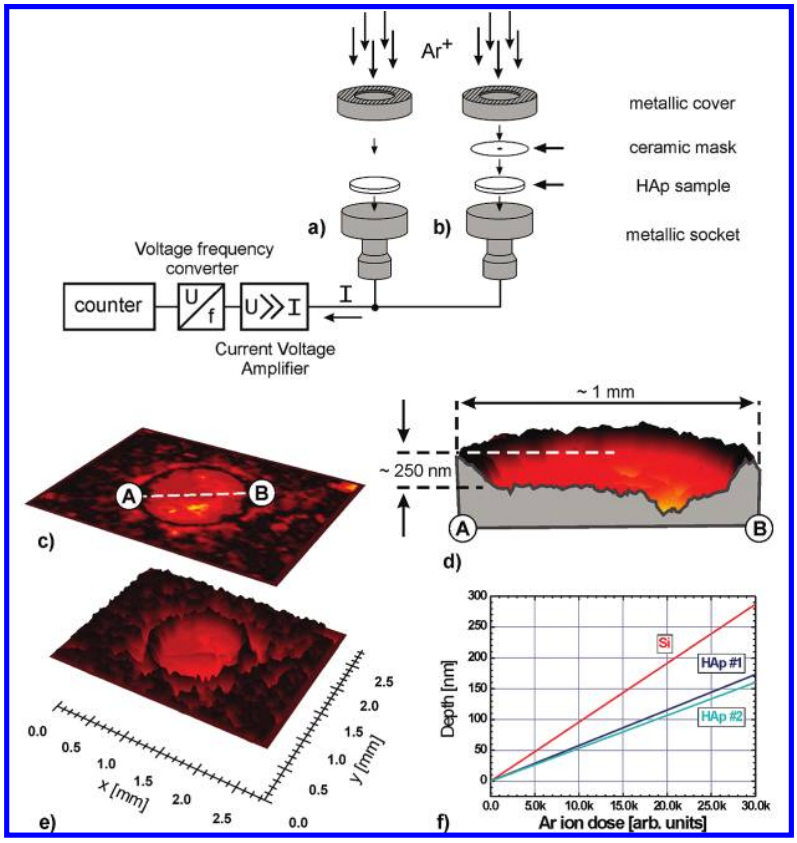

Figure 7. Calibration of Ar etching rate for elemental depth profiling. (a) Setup with nonconducting HAp sample during depth profiling. Only the cross-hatched part of the metallic cover contributes to the measured Ar ion current. (b) Setup with nonconducting HAp sample for calibration. The nonconducting sample is also covered by a nonconducting mask, so that the same area contributes to the measured ion current as in a. (c) Top view of the sputtered hole (after 2 days of Ar ion etching at 4 keV) for a HAp sample as recorded by white light interferometry. (d) Depth profile along the A−B direction in c. (e) 3D image of c. (f) Comparison of the etching rate for a Si and HAp, showing that the etching rate strongly depends on the material.

the total amount of Ar ions that are collected by the metallic ring during an etching period T is then a direct measure for the ablation z of the surface:

$$z = \int_0^T \frac{\mathrm{d}z}{\mathrm{d}t}\mathrm{d}t = c \times \int_0^T \frac{\mathrm{d}n^+}{\mathrm{d}t}\mathrm{d}t = C \times \int_0^T I(\mathrm{Ar}^+)\mathrm{d}t$$

(with c and C describing constants for the specific experimental arrangement; the determination of C will be described below). The last integral represents the overall charge Q that is "counted" by applying a current-to-voltage amplifier, a voltage-to-frequency converter, and a frequency counter, as sketched in Figure 7, and one has

$$\int_0^T I(\mathrm{Ar}^+)\mathrm{d}t \equiv Q$$

(Note: Q includes all fluctuations of the ion current, as, e.g., produced by instabilities of the Ar ion source, and therefore, Q is a measure for the "true" number of Ar ions applied to the sample). Finally, the ablation of the surface for a particular step of Ar ion etching is then given by

$$z = C \times Q$$

The constant C is determined by the calibration setup, as shown in Figure 7b. The HAp sample is now additionally covered by a nonconduction ceramic mask with a 1 mm bore hole to ensure that only a small area of the HAp surface is etched. This area is restricted to 1 mm in diameter just because of instrumental restrictions by the white light interferometer. At this stage, it is important to note that the use of a nonconducting ceramic mask guarantees that in both setups, a and b, the area of the Ar ion collector is the same, namely the area of the metallic ring (the use of a metallic mask during calibration would increase the area of the Ar ion collector, resulting in a large calibration error). For the setup in Figure 7b, the sample is Ar ion etched for several days (with the same parameters of the Ar ion source as applied during depth profiling) with an overall charge Q_0. This procedure results in a hole of 1 mm in diameter and a depth Z_0 of about 250 nm, as determined by white light interferometry (cf. Figure 7c−e). The constant C for calibration of the ablation depth is then simply given by

$$C = \frac{z_0}{Q_0}$$

Finally, for the ablation of the HAp surface by applying an arbitrary Ar ion dose Q, one gets

$$z = \frac{z_0}{Q_0} \times Q$$

Figure 7f shows that the etching rate, as expected, strongly depends on the material. While the etching rate for HAp is nearly the same for two different samples (which gives confidence in our

method), it strongly deviates from that of a Si wafer. Therefore, an elemental depth profiling by combined XPS/Ar ion etching experiments should always be accompanied by a calibration of the etching rate for the particular sample. Other procedures, as, e.g., referring to manufacturers' data sheets, would result in large error bars.

A.2. Calculation of $Ca(OH)_2$, CaF_2, FAp, and HAp Distributions. If the depth distributions for the compounds CaF_2, $Ca(OH)_2$, $Ca_5(PO_4)_3(OH)$, and $Ca_5(PO_4)_3F$ are described by $\alpha(z)$, $\beta(z)$, $\gamma(z)$, and $\delta(z)$, respectively, the relation between the experimental distribution of the elements $n_{ca}(z)$, $n_O(z)$, $n_P(z)$, and $n_F(z)$ and the coefficients $\alpha(z)$, $\beta(z)$, $\gamma(z)$, and $\delta(z)$ is given by the linear equation

$$\begin{aligned} n_{Ca} &= 1\cdot\alpha + 1\cdot\beta + 5\cdot\gamma + 5\cdot\delta \\ n_O &= 0\cdot\alpha + 2\cdot\beta + 13\cdot\gamma + 12\cdot\delta \\ n_P &= 0\cdot\alpha + 0\cdot\beta + 3\cdot\gamma + 3\cdot\delta \\ n_F &= 2\cdot\alpha + 0\cdot\beta + 0\cdot\gamma + 1\cdot\delta \end{aligned}$$

or

$$\begin{pmatrix} n_{Ca} \\ n_O \\ n_P \\ n_F \end{pmatrix} = \begin{pmatrix} 1 & 1 & 5 & 5 \\ 0 & 2 & 13 & 12 \\ 0 & 0 & 3 & 3 \\ 2 & 0 & 0 & 1 \end{pmatrix} \cdot \begin{pmatrix} \alpha \\ \beta \\ \gamma \\ \delta \end{pmatrix}$$

Since the rank of the coefficient matrix is smaller than 4, there is no unambiguous solution. In order to find a solution, we set

$$\varepsilon \equiv \gamma + \delta$$

and, within a first approximation, we introduce a small error in the second line by replacing

$$n_O = 0\cdot\alpha + 2\cdot\beta + 13\cdot\gamma + 12\cdot\delta$$

with

$$n_O = 0\cdot\alpha + 2\cdot\beta + 12.5\cdot\gamma + 12.5\cdot\delta$$

Then, the equation

$$\begin{pmatrix} n_{Ca} \\ n_O \\ n_P \end{pmatrix} = \begin{pmatrix} 1 & 1 & 5 \\ 0 & 2 & 12.5 \\ 0 & 0 & 3 \end{pmatrix} \cdot \begin{pmatrix} \alpha \\ \beta \\ \varepsilon \end{pmatrix}$$

results in the distributions $\alpha(z)$ for CaF_2, $\beta(z)$ for $Ca(OH)_2$, and $\varepsilon(z)$ for the superposition of $Ca_5(PO_4)_3(OH)$ and $Ca_5(OP_4)_3F$ via

$$\gamma(z) + \delta(z) = \varepsilon(z) = \frac{1}{3}\cdot n_P(z)$$

$$\beta(z) = \frac{1}{2}\cdot n_O(z) - \frac{25}{12}\cdot n_P(z)$$

$$\alpha(z) = n_{Ca}(z) + \frac{5}{12}\cdot n_P(z) - \frac{1}{2}\cdot n_O(z)$$

The distribution $\delta(z)$ for FAp can be extracted from the calculated distribution $\alpha(z)$ for CaF_2 and the experimental F distribution $n_F(z)$. Taking the regular stoichiometry for CaF_2, the equation

$$n_F(z) = 2\cdot\alpha(z) + \delta(z)$$

would result in negative values for the FAp distribution $\delta(z)$. With the constraints that $\delta(z)$ must not be negative and that $\delta(z)$ must not exceed the overall FAp/HAp distribution $\gamma(z)$, one gets for the maximal amount of FAp

$$n_F(z) = 1.43\cdot\alpha(z) + \delta(z)$$

and for the minimal amount of FAp

$$n_F(z) = 1.57\cdot\alpha(z) + \delta(z)$$

i.e., the surface is covered by a CaF_x-like material (with $1.43 \le x \le 1.57$) rather than by CaF_2.